Technical University of Denmark

DTU

All-polymer photonic crystal slab sensor

Hermannsson, Pétur Gordon; Sørensen, Kristian Tølbøl; Vannahme, Christoph; Smith, Cameron; Klein, Jan J. ; Russew, Maria-Melanie ; Grützner, Gabi ; Kristensen, Anders

DTU Library
Technical Information Center of Denmark

All-polymer photonic crystal slab sensor

Pétur G. Hermannsson,[1] **Kristian T. Sørensen,**[1] **Christoph Vannahme,**[1] **Cameron L.C. Smith,**[1] **Jan J. Klein,**[2] **Maria-Melanie Russew,**[2] **Gabi Grützner,**[2] **and Anders Kristensen**[1,*]

[1]*Department of Micro- and Nanotechnology, Technical University of Denmark, Ørsteds Plads, Building 345E, DK-2800 Kgs. Lyngby, Denmark*
[2]*micro resist technology GmbH, Köpenicker Straße 325, DE-12555 Berlin, Germany*
[*]*anders.kristensen@nanotech.dtu.dk*

www.nanotech.dtu.dk/ak

Abstract: An all-polymer photonic crystal slab sensor is presented, and shown to exhibit narrow resonant reflection with a FWHM of less than 1 nm and a sensitivity of 31 nm/RIU when sensing media with refractive indices around that of water. This results in a detection limit of 4.5×10^{-6} RIU when measured in conjunction with a spectrometer of 12 pm/pixel resolution. The device is a two-layer structure, composed of a low refractive index polymer with a periodically modulated surface height, covered with a smooth upper-surface high refractive index inorganic-organic hybrid polymer modified with ZrO_2-based nanoparticles. Furthermore, it is fabricated using inexpensive vacuum-less techniques involving only UV nanoreplication and polymer spin-casting, and is thus well suited for single-use biological and refractive index sensing applications.

References and links

1. S. S. Wang and R. Magnusson, "Theory and applications of guided-mode resonance filters," Appl. Opt. **32**, 2606–2613 (1993).
2. R. Magnusson, M. Shokooh-Saremi, and E. G. Johnson, "Guided-mode resonant wave plates," Opt. Lett. **35**, 2472–2474 (2010).
3. D. W. Dobbs and B. T. Cunningham, "Optically tunable guided-mode resonance filter," Appl. Opt. **45**, 7286–7293 (2006).
4. F. Yang, G. Yen, and B. T. Cunningham, "Voltage-tuned resonant reflectance optical filter for visible wavelengths fabricated by nanoreplica molding," Appl. Phys. Lett. **90**, 261109 (2007).
5. F. Yang, G. Yen, G. Rasigade, J. A. Soares, and B. T. Cunningham, "Optically tuned resonant optical reflectance filter," Appl. Phys. Lett. **92**, 091115 (2008).
6. M. J. Uddin and R. Magnusson, "Efficient guided-mode-resonant tunable color filters," IEEE Photonics Technol. Lett. **24**, 1552–1554 (2012).
7. M. J. Uddin, T. Khaleque, and R. Magnusson, "Guided-mode resonant polarization-controlled tunable color filters." Opt. Express **22**, 12307–15 (2014).
8. C. F. R. Mateus, M. C. Y. Huang, Y. Deng, A. R. Neureuther, and C. J. Chang-Hasnain, "Ultrabroadband mirror using low-index cladded subwavelength grating," IEEE Photonics Technol. Lett. **16**, 518–520 (2004).
9. K. J. Lee, D. Wawro, P. S. Priambodo, and R. Magnusson, "Agarose-gel based guided-mode resonance humidity sensor," IEEE Sens. J. **7**, 409–414 (2007).
10. I. W. Jung, B. Park, J. Provine, R. T. Howe, and O. Solgaard, "Monolithic silicon photonic crystal slab fiber tip sensor," in *IEEE/LEOS International Conference on Optical MEMS and Nanophotonics* (IEEE, 2009), pp. 19–20.

11. B. T. Cunningham, B. Lin, J. Qiu, P. Li, J. Pepper, and B. Hugh, "A plastic colorimetric resonant optical biosensor for multiparallel detection of label-free biochemical interactions," Sens. Actuators, B **85**, 219–226 (2002).

12. Y. Nazirizadeh, U. Bog, S. Sekula, T. Mappes, U. Lemmer, and M. Gerken, "Low-cost label-free biosensors using photonic crystals embedded between crossed polarizers," Opt. Express **18**, 19120–19128 (2010).

13. O. Levi, M. M. Lee, J. Zhang, V. Lousse, S. R. J. Brueck, S. Fan, and J. S. Harris, "Sensitivity analysis of a photonic crystal structure for index-of-refraction sensing," Proc. SPIE **6447**, 64470P (2007).

14. L. L. Chan, S. L. Gosangari, K. L. Watkin, and B. T. Cunningham, "A label-free photonic crystal biosensor imaging method for detection of cancer cell cytotoxicity and proliferation," Apoptosis **12**, 1061–1068 (2007).

15. S. Kaja, J. D. Hilgenberg, J. L. Collins, A. A. Shah, D. Wawro, S. Zimmerman, R. Magnusson, and P. Koulen, "Detection of novel biomarkers for ovarian cancer with an optical nanotechnology detection system enabling label-free diagnostics," J. Biomed. Opt. **17**, 081412–1 (2012).

16. W. Chen, K. D. Long, M. Lu, V. Chaudhery, H. Yu, J. S. Choi, J. Polans, Y. Zhuo, B. A. C. Harley, and B. T. Cunningham, "Photonic crystal enhanced microscopy for imaging of live cell adhesion," Analyst **138**, 5886–5894 (2013).

17. Y. Nazirizadeh, J. Reverey, U. Geyer, U. Lemmer, C. Selhuber-Unkel, and M. Gerken, "Material-based three-dimensional imaging with nanostructured surfaces," Appl. Phys. Lett. **102**, 011116 (2013).

18. S. Fan and J. D. Joannopoulos, "Analysis of guided resonances in photonic crystal slabs," Phys. Rev. B **65**, 235112 (2002).

19. T. Khaleque, M. J. Uddin, and R. Magnusson, "Design and fabrication of broadband guided-mode resonant reflectors in TE polarization," Opt. Express **22**, 12349–12358 (2014).

20. C. Ge, M. Lu, S. George, T. A. Flood Jr., C. Wagner, J. Zheng, A. Pokhriyal, J. G. Eden, P. J. Hergenrother, and B. T. Cunningham, "External cavity laser biosensor," Lab Chip **13**, 1247–1256 (2013).

21. S. S. Wang, R. Magnusson, J. S. Bagby, and M. G. Moharam, "Guided-mode resonances in planar dielectric-layer diffraction gratings," J. Opt. Soc. Am. A **7**, 1470–1474 (1990).

22. D. Rosenblatt, A. Sharon, and A. A. Friesem, "Resonant grating waveguide structures," IEEE J. Quantum Electron. **33**, 2038–2059 (1997).

23. Y. Nazirizadeh, U. Lemmer, and M. Gerken, "Experimental quality factor determination of guided-mode resonances in photonic crystal slabs," Appl. Phys. Lett. **93**, 261110 (2008).

24. A. Yariv and P. Yeh, *Photonics: Optical Electronics in Modern Communications*, 6th ed. (Oxford University Press, 2006).

25. A. Sharon, D. Rosenblatt, and A. A. Friesem, "Resonant grating–waveguide structures for visible and near-infrared radiation," J. Opt. Soc. Am. A **14**, 2985–2993 (1997).

26. T. Khaleque, H. G. Svavarsson, and R. Magnusson, "Fabrication of resonant patterns using thermal nano-imprint lithography for thin-film photovoltaic applications," Opt. Express **21**, A631–641 (2013).

27. Y. Nazirizadeh, F. von Oertzen, K. Plewa, N. Barié, P.-J. Jakobs, M. Guttmann, H. Leiste, and M. Gerken, "Sensitivity optimization of injection-molded photonic crystal slabs for biosensing applications," Opt. Mater. Express **3**, 556–565 (2013).

28. Y. Zhuo, H. Hu, W. Chen, M. Lu, L. Tian, H. Yu, K. D. Long, E. Chow, W. P. King, S. Singamaneni, and B. T. Cunningham, "Single nanoparticle detection using photonic crystal enhanced microscopy," Analyst **139**, 1007–1015 (2014).

29. P. G. Hermannsson, C. Vannahme, C. L. C. Smith, and A. Kristensen, "Absolute analytical prediction of photonic crystal guided mode resonance wavelengths," Appl. Phys. Lett. **105**, 071103 (2014).

30. T. Tamir and S. Peng, "Analysis and design of grating couplers," Appl. Phys. **14**, 235–254 (1977).

31. I. M. White and X. Fan, "On the performance quantification of resonant refractive index sensors," Opt. Express **16**, 1020–1028 (2008).

1. Introduction

Optical resonant gratings based on guided mode resonance (GMR) have proven to be a versatile tool within the field of applied optics. In addition to providing means for novel optical elements, such as wavelength selective mirrors, polarizers [1], waveplates [2], tunable filters [3–7] and ultrabroadband mirrors [8], such resonant gratings have increasingly found their way into a myriad of different sensing applications, such as chemical and environmental sensing [9, 10], label-free biosensing [11–13], cancer screening [14, 15], photonic crystal enhanced microscopy [16] and three dimensional imaging [17]. These resonant gratings, referred to here as photonic crystal slabs (PCS) [18], but also known as guided mode resonance filters or reflectors [1, 19] and photonic crystal resonant reflectors [20] in the literature, are essentially slab waveguides in which the high refractive index waveguide core is in some way periodically modulated, such as by refractive index or thickness, and surrounded by cladding media of lower refractive

indices [1, 18]. The periodically modulated waveguide core is able to sustain quasi-guided or leaky waveguide modes, which couple to the far field [21]. When under the illumination of out-of-plane incident light, these quasi-guided modes can be excited within the core. However, due the periodic nature of the core, the light in these modes is continually de-coupled out of the structure where it interferes with both the transmitted and reflected light. At a certain resonance wavelength, the de-coupled light interferes destructively with the transmitted light, resulting in highly efficient resonant reflection for a given wavelength interval [22]. The linewidth, i.e. quality factor, of the reflected interval depends on the rate of de-coupling (lifetime) of the quasi-guided mode, with lower rates of de-coupling (longer lifetimes) leading to narrower linewidths [18, 23, 24]. When the period of the modulation is smaller than the wavelength of the incident light, reflection efficiencies of up to 100% are predicted by theory, but due to factors such as material absorption and fabrication imperfections, the reflection efficiency is reduced. The incident light can excite both transverse-electric (TE) and transverse-magnetic (TM) modes, depending on whether the polarization is perpendicular to or parallel to the grating direction, respectively. Analogously to unmodulated slab waveguides, the intensity of the quasi-guided modes reaches maximum within the waveguide core, and decays exponentially into the cladding regions. Any change in refractive index that occurs in the cladding leads to a change in the guided mode, which manifests itself as a wavelength shift of the resonantly reflected interval. As an example, in label-free biosensing, analytes are immobilized at the waveguide surface, and the evanescent field of the waveguide mode can be used to selectively probe the change in refractive index which occurs on immobilization.

PCSs are commonly fabricated by patterning a low refractive index substrate material by either direct photo- or electron beam lithography [7, 25], or by replication, such as nanoimprint lithography [26], nanoreplication [11] or injection molding [27]. This is then typically followed by the deposition of a layer of a high refractive index material, such as titanium dioxide [28], tantalum pentaoxide [17] or silicon nitride [7, 11], all of which require a vacuum-deposition process.

In this paper, an all-polymer PCS sensor fabricated in a vacuum-less process using UV nanoreplication and polymer spin-casting is presented, which exhibits sharp resonant reflection with a low detection limit and a flat sensing surface. Due to the inexpensive fabrication cost of this PCS sensor, it is highly suitable for high throughput industrial production, and thus ideal for single-use biological and refractive index sensing applications.

2. Device and concept

The polymer PCS investigated here is shown schematically in Fig. 1. It comprises a low refractive index polymer (n_L, LRI) with a periodic surface height modulation of t_g, period $\Lambda = 384$ nm, protrusion duty cycle d, and is covered with a high refractive index polymer (n_H, HRI) which fills the grooves and serves as the waveguide layer. The surface of the HRI layer is at a distance t_f from the LRI polymer and is exposed to a superstrate of bulk refractive index n, referred to here as the sensing region. When illuminated from below with broadband light at normal incidence, the PCS sensor will reflect a narrow wavelength peak corresponding to the refractive index of the medium in the sensing region.
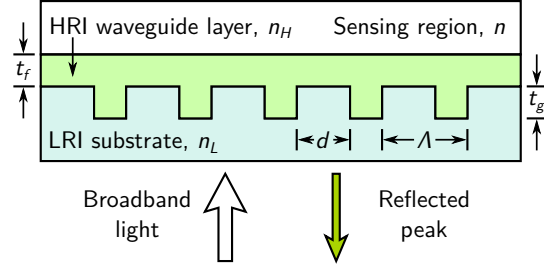

Fig. 1. A schematic illustration of the polymer photonic crystal slab sensor. The device is composed of a low refractive index polymer with a periodically modulated surface height, covered with a layer of the high refractive index polymer OrmoClear® HI01 XP, which in turn is exposed to a sensing region with a bulk refractive index of n.

The peak wavelengths of the resonant reflections can be calculated using an iterative computational model, in which the PCS is modeled as a slab waveguide with an effective core thickness t, where the propagation constant is set to the second order Bragg condition [29]:

$$\beta = 2\pi/\Lambda \tag{1}$$

For TE-polarized guided modes in an asymmetric dielectric slab waveguide, the following mode condition must be satisfied [24]:

$$\tan(ht) = \frac{p+q}{h(1-pq/h^2)} \tag{2}$$

where

$$h = \sqrt{n_H^2 k_0^2 - \beta^2}, \qquad q = \sqrt{\beta^2 - n^2 k_0^2}, \qquad p = \sqrt{\beta^2 - n_L^2 k_0^2}. \tag{3}$$

By solving Eqs. (1)-(3) for k_0, the resonance wavelength λ_R can then be obtained via $\lambda_R = 2\pi/k_0$. In order to obtain the most accurate results, this approach requires that the dispersion of the materials comprising the PCS be taken into account, using e.g. an iterative approach as discussed in Ref. [29]. The dispersion profiles of the LRI and HRI polymers were thus measured using variable angle spectroscopic ellipsometry, the results of which are shown in Fig. 2(a). Using this data and the model described above, the resonance wavelength λ_R of reflected peaks associated with TE-polarized modes was calculated as a function of refractive index in the sensing region n and waveguide layer thickness t. For each given effective thickness t, the resonance shift with respect to air $(n = 1)$ was calculated as a function of n via

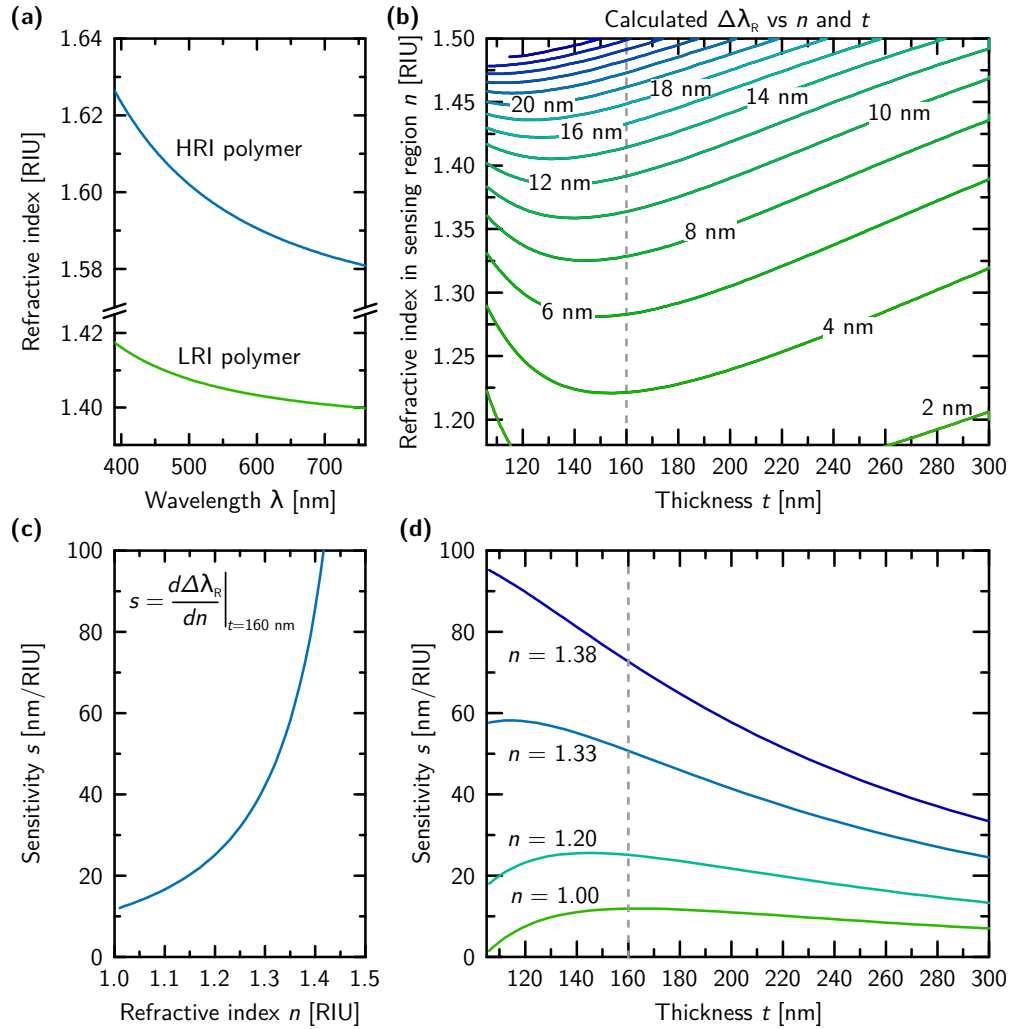$$\Delta\lambda_R(n,t) = \left[\lambda_R(n) - \lambda_R(n=1)\right]_t \tag{4}$$

Fig. 2. (a) The refractive index dispersion of the two polymers from which the PCS sensor is made: Efiron PC-409 (LRI), and OrmoClear® HI01 XP (HRI). (b) The calculated resonance peak shift associated with TE-polarized guided modes as a function of effective waveguide thickness t and sensing region refractive index n. (c) An example of a calculated resonance peak sensitivity for the case of $t = 160$ nm, obtained along the dashed line in panel (b). (d) The calculated sensitivity of resonance peaks associated with TE-polarized modes for four different refractive indices n in the PCS sensing region.

The results are shown in Fig. 2(b). From this data, the sensitivity of the device, as defined by

$$s = \frac{d\Delta\lambda_\mathrm{R}}{dn}\bigg|_t \qquad (5)$$

was calculated as a function of refractive index in the sensing region n. Figure 2(c) shows an example of this for the case of $t = 160$ nm, obtained along the dashed line in Fig. 2(b). Figure 2(d) shows the calculated sensitivity as a function of t for four different sensing region refractive indices. When exposed to air ($n = 1.0$), the minimum effective waveguide layer thickness capable of sustaining a guided mode and thus exhibiting resonant reflection is $t = 106$ nm. For the case of water ($n = 1.33$) the minimum thickness is $t = 64$ nm, and the sensitivity takes a maximum of $s = 58$ nm/RIU at a thickness of $t = 114$ nm. The sensitivity curve for water is quite tolerant to changes in effective waveguide thickness, varying only by a factor of two in the interval $t = (100 - 250)$ nm. Refractive indices between $n = 1.33$ and $n = 1.38$ are of particular interest, as most biosensing takes place in this refractive index range, typically in aqueous solutions containing cells, proteins, etc. Here, the presence of biological agents or the occurrence of biological events is typically associated with very small changes in refractive index, highlighting the importance of understanding how the sensitivity of PCS sensors varies with refractive index n and how it can be optimized by tuning the waveguide layer thickness t.

Since the thickness of the HRI layer in the PCS sensor varies periodically in the guiding direction, it cannot be described directly by the model's effective thickness parameter t, which is constant. However, t can be estimated by the grating's modulation height t_g and film thickness t_f via $t = at_f + b(t_f + t_g)$, where $a, b \in]0, 1[$ are constants that depend on the geometry and duty cycle of the grating. For example, for a perfect binary grating with a protrusion duty cycle d, $a = d$ and $b = (1 - d)$. In general, $t > t_f$, and thus measurements will correspond to the model for values of t greater than t_f. However, as a tool to guide the fabrication of the polymer PCS sensor, it is clear from the simulation results in Fig. 2(d) that the sensor exhibits optimum sensitivity for aqueous and biological sensing applications for film thicknesses t_f of the order of 100 nm, and then drops off monotonously with increasing thickness.

3. Device fabrication and characterization

The polymer PCS sensor was fabricated by UV nanoreplication and polymer spin-casting, as shown in Fig. 3. A silicon master was patterned by electron beam lithography and contained a 2×2 mm one-dimensional, linear grating area with a period of $\Lambda = 384$ nm and a protrusion duty cycle of 25%. The master was anti-stiction coated with a thin layer of perfluorodecyltrichlorosilane (FDTS) using molecular vapor deposition. Placing the master face-up, a droplet of UV curable, low refractive index (LRI, 1.40 RIU at 589 nm), solvent-free polymer (Efiron PC-409, SSCP Co., Ltd.) was dispensed onto the structured area of the master. A borosilicate glass wafer was placed on top of the LRI polymer, sealing it between the master and the glass, where the joint effect of the weight of the glass and capillary forces caused the LRI polymer to spread out and form an even ~ 30 μm layer. After curing the LRI polymer with ultra-violet (UV) light through the glass, the stack was flipped over and the silicon master separated from the LRI polymer, leaving it on the glass. A solution of a high refractive index (HRI, 1.59 RIU at 589 nm) inorganic-organic hybrid polymer modified with ZrO_2-based nanoparticles (OrmoClear® HI01 XP, micro resist technology GmbH) in the polymer thinner ma-T 1050 (25% weight fraction) was prepared and spun onto the cured LRI surface at 2000 RPM, followed by a 10 minute bake-out at 100°C and 10 minutes of UV curing. Due to oxygen in the ambient atmosphere leading to partial quenching of the polymerization of the HRI polymer, a layer of uncured polymer at the surface was rinsed off with isopropanol. In order to estimate the HRI polymer thickness t_f, a silicon wafer was spun with the same HRI

polymer solution and processed identically, yielding a value of $t_f = 180$ nm as ascertained by ellipsometry and profilometry.

(a) Nanostructured silicon master

(b) Low refractive index polymer

(c) Glass wafer

(d) UV curing

(e) Flip structure

(f) Separate master
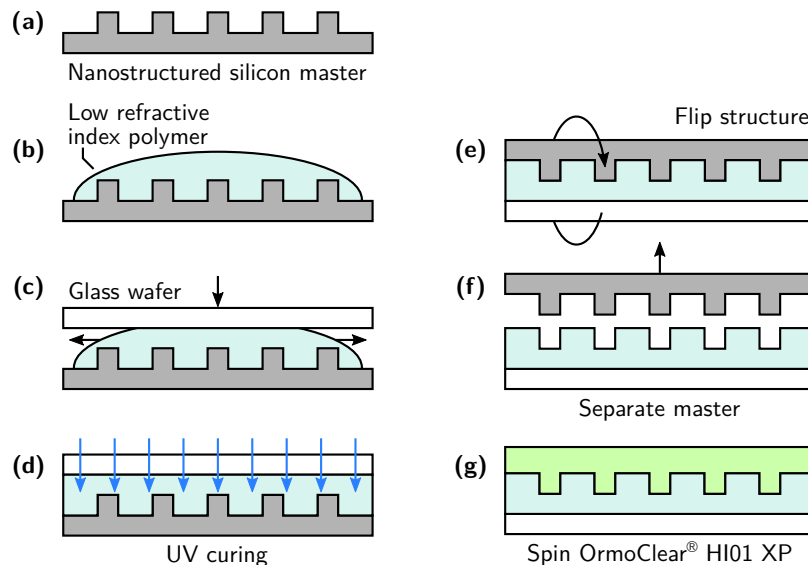
(g) Spin OrmoClear® HI01 XP

Fig. 3. Fabrication of the polymer PCS sensor. (a) Nanostructured silicon master. (b) Dispensing of a low refractive index UV curable polymer onto the master. (c) Sealing of the polymer between the master and a glass wafer. (d) UV curing of the polymer. (e) Flipping over of the stack. (f) Separation and removal of the master. (g) Spinning of the high refractive index polymer OrmoClear® HI01 XP. Not shown: bake-out, UV curing of the high refractive index polymer, and removal of inhibition layer.

The topography of the LRI and HRI polymer surfaces were measured with atomic force microscopy (AFM) using a high aspect ratio tip, i.e. after the silicon master removal and after the spin-coating steps, respectively. Figure 4(a) shows a 3D surface scan of the nanoreplicated LRI polymer, and Fig. 4(b) shows the AFM scan profiles for both LRI and HRI polymer surfaces, as averaged over 30 parallel line scans. The side-walls of the LRI layer grating protrusions are not perfectly vertical, and are furthermore less vertical than the grating protrusions of the silicon master. This is thought to be a result of the nanoreplication process itself, either due to relaxation of the cured polymer, or due to deformation of the polymer upon release of the silicon master. However, the trapezoidal shape of the grating protrusions is not believed to negatively impact the performance of the sensor. On the contrary, it has been shown that guided modes in grating waveguides with trapezoidal protrusion shapes generally exhibit lower de-coupling rates than those in square ones [30], and thus exhibit higher resonance quality factors. It is also worth noting that the surface of the HRI polymer does not conform to the grating topography, but rather is flat. This may be a considerable advantage in biological sensing of surface-immobilized analytes, as it excludes any influence of the surface topography on the analyte. Finally, Fig. 4(c) shows a scanning electron micrograph of the nanoreplicated LRI polymer, obtained before the application of the HRI polymer.

The PCS sensor was fabricated from these two particular polymers primarily on account of their suitable refractive indices and chemical properties. UV nanoreplication requires the use of a solvent-free and UV curable polymer, and for the current application, the polymer must furthermore have a low refractive index. Efiron PC-409 satisfies each of these criteria. OrmoClear® HI01 XP was chosen for the waveguide layer due to its high refractive index and
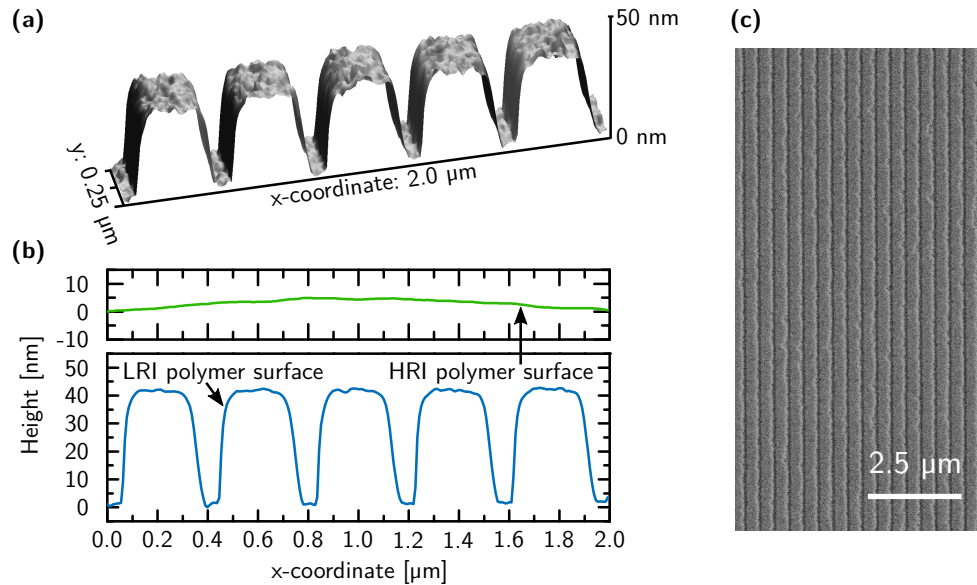
Fig. 4. Characterization of the polymer PCS sensor. (a) A 3D AFM scan of the surface of the low refractive index polymer after the removal of the silicon master. (b) AFM traces of the low refractive index polymer surface and the surface of the high refractive index polymer. Both are averaged over 30 parallel line scans. (c) Scanning electron micrograph of the nanostructured low refractive index polymer surface.

simple processing in terms of diluting and spinning into thin films. Furthermore, it is highly transparent in the visible regime and mechanically rigid after curing.

The silicon master is highly durable when used in UV nanoreplication. In contrast to conventional nanoimprint lithography, the master is neither subjected to high temperatures nor high pressures. Furthermore, the stamp is only exposed to a solvent-free polymer, which does not cause the anti-stiction coating to deteriorate. The authors of the present work have performed over 90 nanoreplications with a single master without degradation in the quality factor of the resonantly reflected wavelength peak.

4. Experimental measurements and results

The reflected spectra from the fabricated PCS sensor were measured by illumination at normal incidence from the back-side, using the experimental setup shown in Fig. 5. Light from a high-brightness, broadband laser-driven light source (Energetiq EQ-99XFC) is fed to the setup via an optical fiber, collimated with a fiber collimator, and then focused with a lens and reflected into a microscope objective by a beamsplitter. The light then emerges collimated from the other side of the objective and illuminates the PCS sensor at normal incidence. The reflected light travels backwards through the objective and beamsplitter and is then simultaneously focused by a microscope tube lens onto the slit of an imaging spectrometer and a camera (CCD A) via a polarizing beamsplitter. The polarizing beamsplitter reflects *s*-polarized light to the spectrometer, while *p*-polarized light passes through it to the camera, where it is captured, transmitted to a computer and used for visual inspection of the PCS sensor and sample positioning. Therefore, when the PCS is oriented as shown here, resonant reflections associated with TE-polarized guided modes correspond to an *s*-polarization and are thus

reflected to the spectrometer, while resonant reflections associated with TM-polarized guided modes correspond to a *p*-polarization and are transmitted towards the camera. Conversely, in order to measure TM-polarized resonantly reflected light with the spectrometer instead, the PCS can be rotated by 90°, in which case the TE-polarized resonantly reflected light will be directed to the camera. The imaging spectrometer contains a diffraction grating with 1800 lines/mm and projects the input spectrum onto a second camera (CCD B) with a resolution of 12 pm/pixel. The camera is further connected to a computer, where the spectrum is acquired and analyzed.
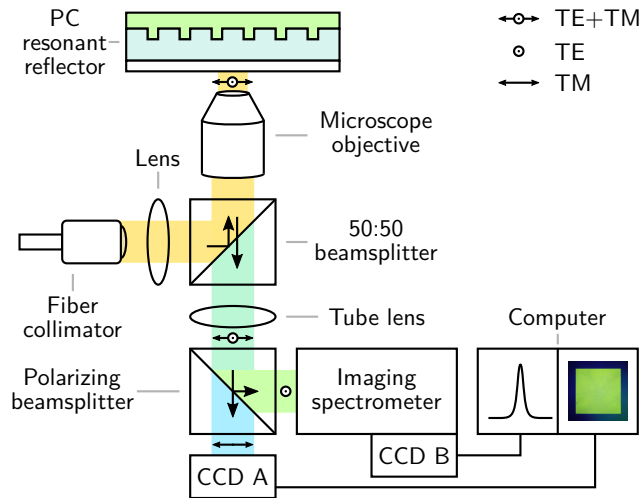

Fig. 5. Experimental setup for measuring resonantly reflected light from the polymer PCS sensor. The structure may exhibit resonant reflection associated with both TM and TE-polarized guided modes. The TM-polarized reflected light is directed to a camera (CCD A) where it is used for visual inspection and sample positioning, whereas the TE-polarized reflected light is directed to an imaging spectrometer and projected onto a second camera for spectral analysis (CCD B).

Using this setup, the reflected TE-polarized resonance peak from the fabricated PCS sensor was measured as a function of refractive index in the sensing region, corresponding to air, deionized water, glycerol, and several dilutions of glycerol in water with weight fractions ranging between 15% and 80%. Figure 6(a) shows an example of two measured spectra, corresponding to the cases of air and deionized water. The resonance peaks are characterized by very narrow, asymmetric peaks with a full width at half maximum intensity (FWHM) of less than 0.9 nm. This narrow resonant linewidth is a direct result of the relatively low refractive index contrast between the substrate and the waveguide layer as well the low grating perturbation [18], both of which lead to long quasi guided mode lifetimes. At shorter wavelengths with respect to the primary reflected peak, a low-intensity secondary peak is visible. However, for the purpose of tracking refractive index changes in the sensing region, this secondary peak is not of concern. Similarly, the TM-polarized reflection was measured, but was found to be barely discernible from the background noise, and is thus not discussed further. Figure 6(b) shows the measured resonance peak wavelength shift with respect to air as a function of refractive index in the sensing region, compared to the model results for the case of $t = 253$ nm (c.f. Fig. 2(b)). The results show clear agreement with the model. Figure 6(b) further shows the sensitivity of the device as a function of refractive index in the sensing region n, calculated using Eq. (5). At a refractive index of $n = 1.33$, the sensitivity of the device is obtained to be $s = 31$ nm/RIU, increasing quickly to $s = 43$ nm/RIU for $n = 1.38$ RIU.
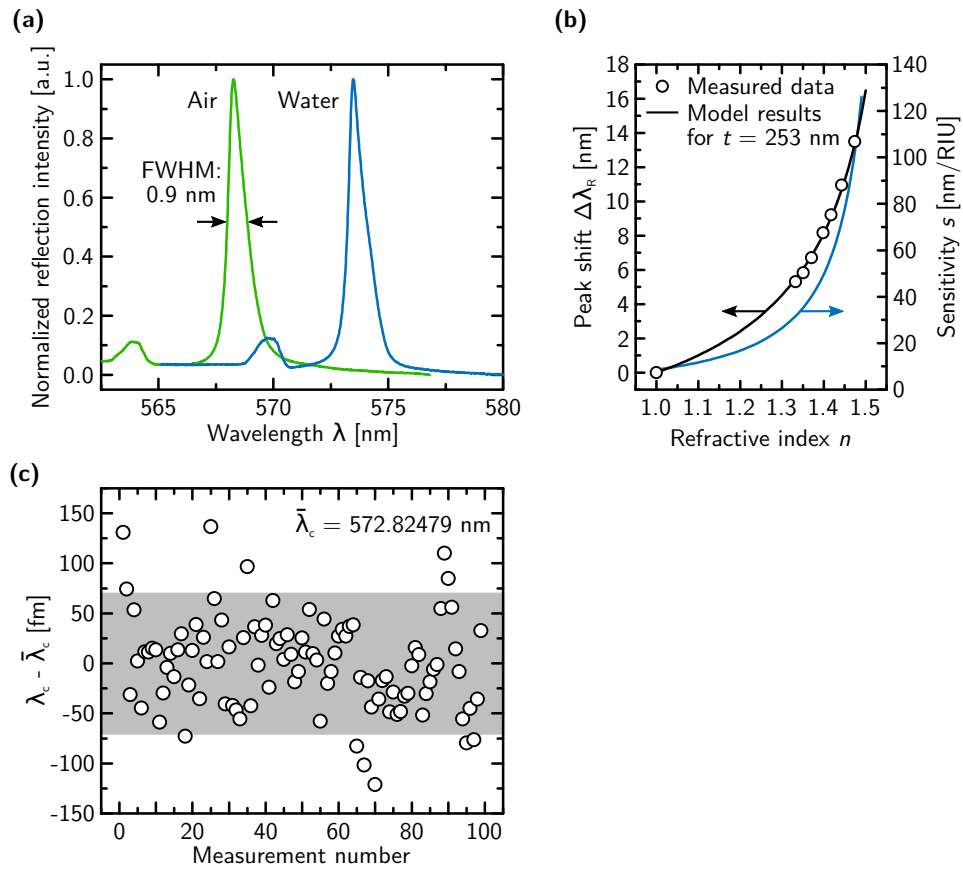
Fig. 6. (a) Acquired resonance spectra of TE polarized reflected light from the polymer PCS sensor when covered with air and deionized water. (b) Measured peak wavelength shift $\Delta\lambda_R$ as a function of refractive index in the sensing region n, compared to simulation results for the case of $t = 253$ nm. The sensitivity of the device s as a function of n, obtained from the slope of $\Delta\lambda_R(n)$ is further shown on the right axis. (c) A series of 100 measurements of the center wavelength λ_c, shown relative to the mean $\bar{\lambda}_c$. The gray area represents three standard deviations of λ_c.

It should be noted that while the presented PCS sensor exhibits a sensitivity lower than those of silicon nitride and titanium dioxide-based structures, this parameter alone does not fully describe the performance of the sensor as it ignores the importance of the resonance linewidth. Instead, the device's performance is better described by its detection limit, which quantifies the smallest refractive index change that the sensor can measure [31]:

$$\mathrm{DL} = \frac{3\sigma}{s} \tag{6}$$

where σ is the standard deviation of the resonance peak wavelength obtained from measurements and is dependent on the linewidth. Therefore, with deionized water in the sensing region, a series of 100 measurements of the TE-polarized reflected peak were acquired, each with an integration time of 100 ms. For each measurement, the center wavelength λ_c was determined using a center of mass calculation:

$$\lambda_\mathrm{c} = \frac{\sum_{i=n}^{m} \lambda_i I_i}{\sum_{i=n}^{m} I_i} \tag{7}$$

where I_i is the measured intensity at a wavelength of λ_i in spectral position i, and the integers n and m are chosen such that the calculation encompasses the primary peak only. The results are shown in Fig. 6(c), and the standard deviation of λ_c was determined to be $\sigma = 4.6 \times 10^{-5}$ nm. This yields a detection limit of 4.5×10^{-6} RIU for the polymer PCS sensor when sensing materials with refractive indices around that of water. For biological sensing applications with refractive indices around $n = 1.38$ RIU, the detection limit can be expected to be even lower, or 3.2×10^{-6} RIU.

5. Summary and discussion

An all-polymer photonic crystal slab sensor fabricated by inexpensive vacuum-less techniques involving only UV nanoreplication and polymer spinning has been presented. The structure is shown to exhibit sharp resonant TE-polarized reflection with a FWHM of less than 0.9 nm, a sensitivity of 31 nm/RIU and a detection limit of 4.5×10^{-6} RIU, for sensing materials with refractive indices close to that of water. The sensitivity of the device could in principle be optimized by spinning a thinner layer of the high refractive index waveguide material. This should lead to a higher sensitivity, but possibly also a broadening of the resonance peak, so layer thickness optimization must be carefully considered in order to improve the detection limit. In any case, such a polymer PCS sensor is well-suited for high-throughput industrial production due to the fabrication methods and materials involved, and is therefore ideal for single-use biological and other refractive index sensing applications.